PAPER

Selective growth of chirality-enriched semiconducting carbon nanotubes by using bimetallic catalysts from salt precursors†

Xiulan Zhao,[a] Feng Yang,[a] Junhan Chen,[a] Li Ding,[a] Xiyan Liu,[a] Fengrui Yao,[b] Meihui Li,[a] Daqi Zhang,[a] Zeyao Zhang,[a] Xu Liu,[a] Juan Yang,[a] Kaihui Liu [ID][b] and Yan Li [ID] *[a]

Bimetallic catalysts play important roles in the selective growth of single-walled carbon nanotubes (SWNTs). Using the simple salts $(NH_4)_6W_7O_{24}\cdot6H_2O$ and $Co(CH_3COO)_2\cdot4H_2O$ as precursors, tungsten-cobalt catalysts were prepared. The catalysts were composed of W_6Co_7 intermetallic compounds and tungsten-dispersed cobalt. With the increase of the W/Co ratio in the precursors, the content of W_6Co_7 was increased. Because the W_6Co_7 intermetallic compound can enable the chirality specified growth of SWNTs, the selectivity of the resulting SWNTs is improved at a higher W/Co ratio. At a W/Co ratio of 6 : 4 and under optimized chemical vapor deposition conditions, we realized the direct growth of semi-conducting SWNTs with the purity of ~96%, in which ~62% are (14, 4) tubes. Using salts as precursors to prepare tungsten-cobalt bimetallic catalysts is flexible and convenient. This offers an efficient pathway for the large-scale preparation of chirality enriched semiconducting SWNTs.

Introduction

Single-walled carbon nanotubes (SWNTs) have shown great potential in nanoelectronics,[1–4] energy,[5,6] biotechnology,[7] and other fields.[8] However, many applications require SWNTs with specific properties. For example, pure semiconducting SWNTs are critically demanded in the nanoelectronic devices.[1] Besides, chirality-specific SWNTs have been demonstrated to present superior performance in many applications such as high-resolution multicolor biological imaging,[9,10] high efficiency photovoltaic processes,[11–13] and photocatalytic water splitting.[14] However, the controllable preparation of SWNTs is still very challenging and requires more efforts.[15–18]

Metal catalysts play important roles in the synthesis of SWNTs by chemical vapor deposition (CVD). Bimetallic catalysts have been widely used to grow SWNTs with narrow diameter and/or chirality distributions.[16,19] For instance,

SWNTs with a large abundance of (6, 5) tubes up to 55% were achieved using CoMo,[20,21] FeCu,[22] FeRu,[23] CoCu[24] and so on. By tuning the CVD conditions, SWNT samples with increased content of (7, 6) or (8, 4) were also selectively obtained by using bimetallic catalysts.[22,23] It was speculated that Fe or Co acts as the catalytic component, and the other metals anchor the active metal nanoparticles to make them stable and uniform, which is beneficial to the selective growth of SWNTs.[24,25]

Recently, we developed W_6Co_7 intermetallic catalysts for the chirality selective growth of SWNTs. Distinctly different from the previously reported bimetallic catalysts, W_6Co_7 present well-defined unique crystal structures and high melting points, enabling the template growth of SWNTs with designed structures.[16,26] By using W_6Co_7 catalysts, we realized the growth of (12, 6), (16, 0), and (14, 4) tubes with the purity of 92%, 79%, and 97%, respectively.[26–28] In these studies, the formation of W_6Co_7 intermetallic compounds is essential for the chirality-specified growth of SWNTs. Therefore, a kind of molecular cluster containing W and Co was used as the catalyst precursor. Actually, conventional W-based bimetallic catalysts have also exhibited their feasibility in the selective growth of SWNTs. For instance, sputtered Co–W catalysts have been used to grow (12, 6)-dominated SWNTs[29] and W-supported Ni catalysts have shown to be very robust in growing SWNTs with narrow diameter distribution.[30] These results indicate that the W–Co system should be superior in the controllable synthesis

[a]*Beijing National Laboratory for Molecular Science, Key Laboratory for the Physics and Chemistry of Nanodevices, State Key Laboratory of Rare Earth Materials Chemistry and Applications, College of Chemistry and Molecular Engineering, Peking University, Beijing 100871, China. E-mail: yanli@pku.edu.cn*
[b]*State Key Laboratory for Mesoscopic Physics, Collaborative Innovation Center of Quantum Matter, School of Physics, Academy for Advanced Interdisciplinary Studies, Peking University, Beijing 100871, China*
†Electronic supplementary information (ESI) available. See DOI: 10.1039/c7nr07855b

of SWNTs. No matter W_6Co_7 intermetallic compound or W-anchored Co nanoparticles are eventually formed, the controlled growth can be expected. Therefore, using metal salts as catalyst precursors should be convenient and effective.[15,31]

In this study, we used commercially available salts containing W and Co respectively, $(NH_4)_6W_7O_{24} \cdot 6H_2O$ and Co$(CH_3COO)_2 \cdot 4H_2O$, as catalyst precursors. By mixing the two kinds of salts at an optimized W/Co ratio, we realized the direct growth of (14, 4) SWNTs with the purity of ~62% and semiconducting SWNTs with the abundance of ~96%, simultaneously.

Results and discussion

To prepare W–Co bimetallic catalysts, the $(NH_4)_6W_7O_{24} \cdot 6H_2O$ and Co$(CH_3COO)_2 \cdot 4H_2O$ precursor with a W/Co molar ratio of 6/4 was annealed, and then reduced in hydrogen from 800 to 1030 °C. X-ray diffraction (XRD) and transmission electron microscopy (TEM) were used to characterize the prepared catalysts. The diffraction peaks present in the XRD patterns of the catalyst are readily ascribed to W_6Co_7 and W, respectively (Fig. 1a). The scanning transmission electron microscopy-energy dispersive X-ray analysis (STEM-EDX) mapping shows that the W and Co elements are homogeneously mixed in the

nanoparticles (Fig. 1b–d). The observed lattice spacing of the lattice fringes in the high-resolution transmission electron microscopy (HRTEM) image is 0.22 nm (Fig. 1e), which is in good accordance with the (1 0 10) plane distance of W_6Co_7. Both the results of XRD and TEM measurements prove that intermetallic W_6Co_7 catalysts are formed in the W–Co bimetallic catalyst when using $(NH_4)_6W_7O_{24} \cdot 6H_2O$ and Co$(CH_3COO)_2 \cdot 4H_2O$ as precursors. Then we performed the CVD growth of SWNTs on Si/SiO$_2$ substrates using such produced catalysts. The SEM image shows the random SWNTs grown on the Si/SiO$_2$ substrate (Fig. 2a). The high G/D ratio of the SWNTs indicates the high quality of the grown SWNTs (Fig. 2b). The multi-wavelength resonant Raman spectra measurement is a convenient and accurate method for making (n, m) assignments and quantification of the SWNTs.[32] Here, four different lasers with wavelengths of 488, 532, 633, and 785 nm were used to detect the radial breathing mode (RBM) peaks (Fig. 3a–d). The Raman spectra acquired with a 532 nm laser show RBM peaks concentrated around 189 cm^{-1}, which are assigned to (14, 4) tubes according to the Kataura plot.[28,32,33] The fluorescence emission locates at 0.77 eV, which also corresponds to the first (E_{11}) van Hove optical transition energy of the (14, 4) tube (Fig. S1a†).[28] According to the statistics of nearly two hundreds of RBM peaks, the abundance of the (14, 4) SWNTs is estimated to be 62% and the purity of semiconducting SWNTs to be 96% (Fig. 3e). The as-grown SWNTs were transferred onto the Si/SiO$_2$ (thickness: 90 nm) substrate to perform polarization-based optical microscopy.[34] The estimated abundance of (14, 4) tubes based on the peaks averaging at 2.2 eV is 58.3% (Fig. S1b†), which closely matches the value determined from Raman spectra. The diameters (d_t) of the SWNTs are calculated according to the relation $\omega_{RBM} = 239.5/d_t + 5.5$ (Fig. 3f).[32] It shows that the diameters of 96% SWNTs are located in the range of 1.2–1.4 nm with a mean value of 1.30 ± 0.07 nm.

We systematically investigated the effect of the W/Co ratio on the chiral selectivity of the SWNTs. As shown in Fig. 4, the abundance of (14, 4) SWNTs increases with the increase of the W/Co ratio. No selectivity to (14, 4) tubes was observed when using pure Co as catalysts. The content of (14, 4) tubes changes from 9% to 62% when the ratio of W/Co increased from 6/12 to 6/4 (Fig. 4). Since W_6Co_7 has a W/Co stoichio-
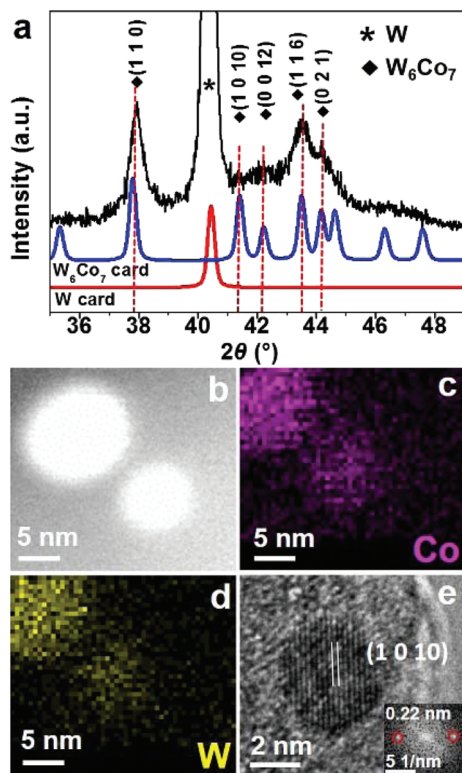

Fig. 1 Characterization of the catalysts prepared at 1030 °C from the salt precursors. (a) XRD patterns. (b) HAADF-STEM image. (c, d) Energy-dispersive X-ray spectroscopy (EDX) elemental mapping of Co and W in the corresponding area in (b). (e) HRTEM image of W_6Co_7 nanoparticles with the inset showing the corresponding fast Fourier transform spectra.
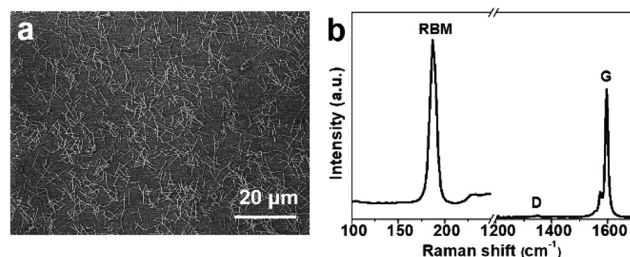
Fig. 2 (a) SEM image of the SWNTs grown on the Si/SiO$_2$ substrate. (b) The typical Raman spectrum of the SWNTs grown under the optimized conditions (excitation wavelength: 532 nm).
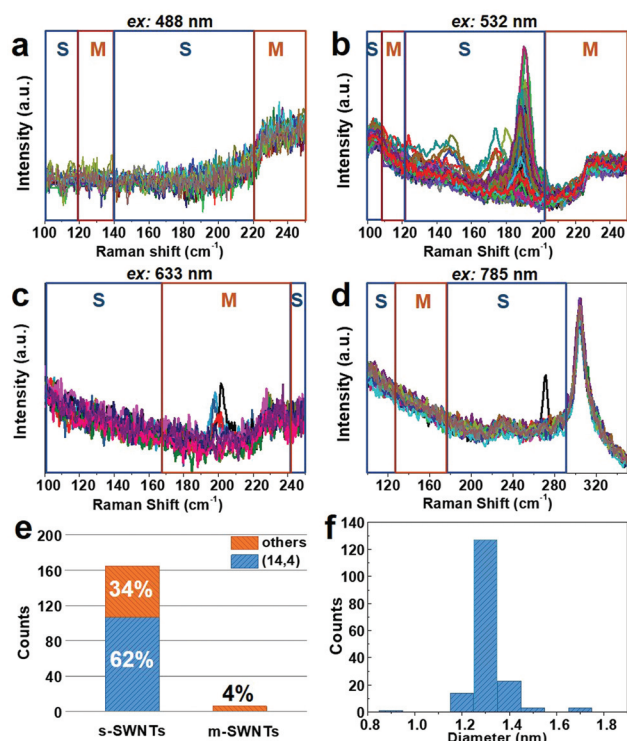
Fig. 3 (a–d) Multi-wavelength Raman spectra of the SWNTs grown under the optimized conditions. Peaks marked with S and M within the rectangles correspond to the semiconducting and metallic SWNTs, respectively. (e) Statistics of the abundance of the (14, 4) SWNTs and semiconducting SWNTs based on the Raman measurements. (f) Statistics of the diameter of the SWNTs based on the Raman measurements.
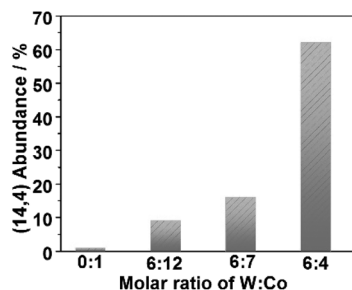

Fig. 4 Selectivity of (14, 4) SWNTs using the catalysts prepared through a catalyst precursor with different W/Co ratios. The selectivity was based on statistics of the RBM peaks in Raman measurements.

metric ratio of 6/7, when the catalyst precursors with a W/Co ratio less than 6/7 were used, the (14, 4) abundance is always low due to the presence of excess Co nanoparticles. When we used the catalyst precursor with the W/Co ratio of 6/7, the abundance of the grown (14, 4) tubes was still low. When the W/Co ratio was 6/4, the purity of the (14, 4) tubes was significantly improved to 62%. This indicates that excess tungsten is needed to effectively 'trap' cobalt into the W_6Co_7 intermetallic compound. Meanwhile, excess tungsten can also disperse the cobalt nanoparticles and make them uniform. However, on

further increasing the W/Co ratio to 6/3, many multi-walled carbon nanotubes (MWNTs) and amorphous carbon were formed. We speculated that tungsten carbides formed and promoted the decomposition of a carbon source to form MWNTs and amorphous carbon.[35–38]

We used X-ray photoelectron spectroscopy (XPS) to further characterize the composition of the resulting catalysts. Fig. 5 shows XPS spectra of the catalysts prepared by three different catalyst precursors in which the W/Co ratios were 6/12, 6/7, and 6/4, respectively. The spectra were recorded around the Co 2p core levels, where the background component was subtracted by the Shirley method. The binding energy peak located at 780.2 eV was attributed to Co $2p_{3/2}$ of CoO, since the metallic Co catalyst was oxidized by exposure to air. The peak at 778.1 eV with a higher intensity was assigned to Co $2p_{3/2}$ of W_6Co_7.[39] The ratios of W_6Co_7/Co calculated from the integrated peak intensity were 1/1.4, 1/1.1, and 1/1.0, respectively. This result indicates that the higher selectivity toward the (14, 4) tubes at a higher W/Co ratio originated from the increased content of W_6Co_7.

We also carefully analysed the catalyst composition after the growth of SWNTs. To perform the XRD measurements, we prepared the silica sphere supported catalysts with the W/Co ratio of 6/4 and then performed the CVD. The W_6Co_7 nanoparticles still existed after the CVD process, but the isolated W and Co were carbonized to W_2C or W_6Co_6C (Fig. 6 and Fig. S2†).
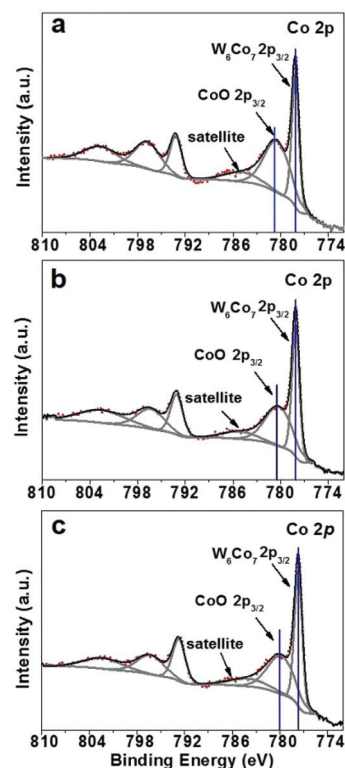
Fig. 5 (a–c) The Co 2p XPS spectrum of the catalysts prepared from W–Co salts with different W/Co ratios: 6/12 (a), 6/7 (b), and 6/4 (c), respectively.
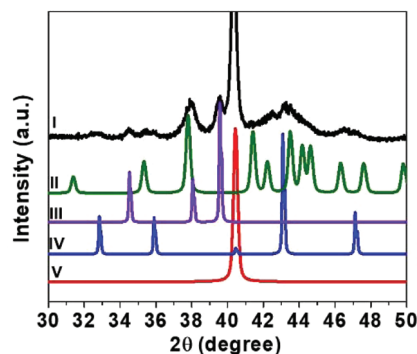
Fig. 6 XRD patterns of the W–Co catalyst supported on the SiO_2 sphere after the CVD process (I) together with the standard cards from the JCPDS database, W_6Co_7 (JCPDS 2-1091) (II), W_2C (JCPDS 20-1315) (III), Co_6W_6C (JCPDS 22-0597) (IV), W (JCPDS 4-0806) (V).

Besides the catalyst structures, the CVD conditions can also affect the chirality distribution of SWNTs.[16,21,40,41] We performed a series of experiments to explore the influence of the ratio of the flow rate of argon though an ethanol bubbler and hydrogen ($EtOH/H_2$) on the chiral-selective growth (Fig. 7). The optimized selectivity to the (14, 4) tube was acquired when the $EtOH/H_2$ ratio was 180/30. The content of metallic SWNTs was decreased from 11% to 4%, when the ratio increased from 150/30 to 180/30. When the $EtOH/H_2$ ratio was further increased to 200/30, the content of metallic tubes was estimated to be 6% (Fig. 7d). The selectivity toward semiconducting nanotubes may originate from two factors. The narrow diameter distribution of 1.2–1.4 nm with enriched semiconducting (14, 4) tubes improved the content of semiconducting SWN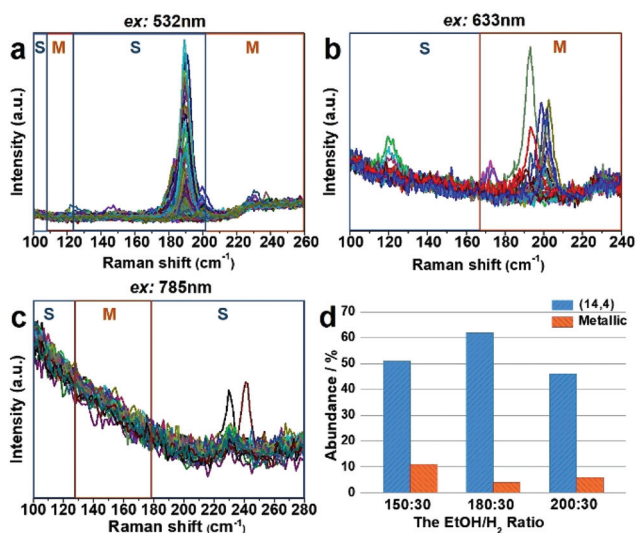Ts. In addition, a small amount of oxygen stored in the bubbler was introduced to the quartz tube reactor by the carrying gas Ar in the growth stage and the metallic SWNTs were etched.[42,43] When both the etching rate of metallic tubes and growth speed of metallic nanotubes were suitable, we could obtain high semiconducting selectivity (Fig. 7d).[44] If we purged the bubbler with 400 sccm Ar for 10 min, and then performed the experiment following the optimal CVD conditions, nevertheless, there was much amorphous carbon resulting, which further proved the existence and etching effect of oxygen (Fig. S3†).

Conclusions

A W–Co bimetallic catalyst is a suitable catalyst system for the controllable growth of SWNTs. We developed a very simple method to prepare W–Co bimetallic catalysts by simply mixing the salts containing tungsten and cobalt as catalyst precursors. Then W–Co bimetallic catalysts containing W_6Co_7 nanoparticles were synthesized through further sintering and reducing the precursor under appropriate conditions. The W–Co ratio significantly influenced the chiral selectivity of the grown SWNTs. Through carefully tuning the W/Co ratio and CVD conditions, we obtained the sample with 96% semiconducting SWNTs including 62% (14, 4) tubes. This feasible method to prepare W–Co bimetallic catalysts will make it possible to realize the large-scale growth of chirality enriched semiconducting SWNTs.

Experimental

Catalyst preparation and SWNT synthesis

10 mL of 15/7 mmol L^{-1} $(NH_4)_6W_7O_{24}$ aqueous solution was dropwise added to 10 mL of 10 mmol L^{-1} $Co(CH_3CO_2)_2$ aqueous solution with stirring. An appropriate amount of acid was added to make the solution weakly acidic. Then this solution was diluted 100 times with ethanol as the precursor solution. Silicon wafers with ~300 nm of silica layer were used as substrates after hydrophilic treatment by piranha solution. The general CVD process was carried out under atmospheric pressure in a 1 inch quartz tube heated by using a horizontal tube furnace. The precursor solution was dropped onto the SiO_2/Si substrates and calcined at 700 °C in air for 5 min. When the air in the system was removed by Ar, H_2 at the flow of 200 cm^3 min^{-1} was introduced to reduce the calcined catalyst precursors using a TPR process from 800 to 1030 °C for 6 min. Afterwards, a flow of 150–200 cm^3 min^{-1} Ar through an ethanol bubbler (in an ice-water bath) and 30–50 cm^3 min^{-1} hydrogen were introduced into the system for 10 min to grow SWNTs at 1030 °C. Finally, the system was cooled down to room temperature under a flow of H_2 and Ar, respectively.

Characterization

We used SiO_2 microspheres (diameter: ~300 nm) as the catalyst support to prepare catalysts for XRD and STEM-EDX characterization. The XRD measurements were performed on a

Fig. 7 (a–c) The multi-wavelength Raman spectra of the SWNTs grown at the $EtOH/H_2$ ratio of 150 : 30. Peaks marked with S and M within the rectangles correspond to the semiconducting and metallic SWNTs, respectively. (d) Statistical chart of the purity of (14, 4) and metallic tubes synthesized at different $EtOH/H_2$ ratios based on the Raman measurements.

DMAX-2400 X-ray diffractometer using monochromatic Cu-Kα radiation (λ = 0.154 nm, 60 kV, 200 mA). Scanning transmission electron microscopy (STEM) and energy-dispersive X-ray analysis (EDX) element mappings were conducted under a high-angle annular dark field (HAADF) mode on an FEI Tecnai F30 microscope operating at 300 kV. The Si_3N_4 thin film (thickness: 5 nm) was used as the support of the catalysts for HRTEM characterization. HRTEM was performed on an FEI Tecnai F20 microscope operating at 200 kV. The X-ray photoelectron spectroscopy (XPS) experiments were performed using an AXIS Supra/Ultra Imaging X-ray Photoelectron Spectrometer. The SEM images of SWNTs were obtained on a Hitachi S4800 SEM operating at 1.0 kV. The Raman spectra of the grown SWNTs were collected with two Jobin Yvon-Horiba LabRam systems: an ARAMIS system for 532, 633, and 785 nm laser excitations, and an HR800 system for 488 nm. The laser beam spot used to collect the Raman signal of the SWNTs was 1 μm in diameter. The Raman spectra using different excitation wavelengths were recorded on the same regions. The photoluminescence spectra of the as-grown suspended SWNTs were collected with a Jobin Yvon-Horiba LabRam system, and an ARAMIS system for 532 nm laser excitation equipped with an InGaAs detector. The optical reflection spectra of carbon nanotubes were acquired using polarization-based microscopy combined with supercontinuum laser illumination developed by Liu and Wang et al. Each spectrum was obtained within 20 s using broadband supercontinuum illumination and a spectrometer equipped with a linear-array charge-coupled device (CCD).

Author contributions

Yan Li and Xiulan Zhao provided the primary idea, designed the experiments, analyzed the results and wrote the manuscript. Xiulan Zhao, Feng Yang, Junhan Chen, Li Ding, Xiyan Liu, Meihui Li, Daqi Zhang, Zeyao Zhang, Xu Liu, Fengrui Yao, Kaihui Liu and Juan Yang performed the experiments and analyzed the results.

Conflicts of interest

There are no conflicts to declare.

Acknowledgements

Notes and references

1 A. D. Franklin, *Nature*, 2013, **498**, 443–444.

2 M. M. Shulaker, G. Hills, N. Patil, H. Wei, H.-Y. Chen, H. S. P. Wong and S. Mitra, *Nature*, 2013, **501**, 526–530.

3 A. D. Franklin, *Science*, 2015, **349**, 2751–2579.

4 J. Yao, Z. Jin, L. Zhong, D. Natelson and J. M. Tour, *ACS Nano*, 2009, **3**, 4122–4126.

5 I. Jeon, K. Cui, T. Chiba, A. Anisimov, A. G. Nasibulin, E. I. Kauppinen, S. Maruyama and Y. Matsuo, *J. Am. Chem. Soc.*, 2015, **137**, 7982–7985.

6 Z. Zhang, L. Wei, X. Qin and Y. Li, *Nano Energy*, 2015, **15**, 490–522.

7 G. Hong, A. L. Antaris and H. Dai, *Nat. Biomed. Eng.*, 2017, **1**, 0010.

8 M. F. L. De Volder, S. H. Tawfick, R. H. Baughman and A. J. Hart, *Science*, 2013, **339**, 535–539.

9 S. Diao, G. Hong, J. T. Robinson, L. Jiao, A. L. Antaris, J. Z. Wu, C. L. Choi and H. Dai, *J. Am. Chem. Soc.*, 2012, **134**, 16971–16974.

10 Y. Yomogida, T. Tanaka, M. Zhang, M. Yudasaka, X. Wei and H. Kataura, *Nat. Commun.*, 2016, **7**, 12056.

11 R. M. Jain, R. Howden, K. Tvrdy, S. Shimizu, A. J. Hilmer, T. P. McNicholas, K. K. Gleason and M. S. Strano, *Adv. Mater.*, 2012, **24**, 4436–4439.

12 D. J. Bindl and M. S. Arnold, *J. Phys. Chem. C*, 2013, **117**, 2390–2395.

13 C. M. Isborn, C. Tang, A. Martini, E. R. Johnson, A. Otero-de-la-Roza and V. C. Tung, *J. Phys. Chem. Lett.*, 2013, **4**, 2914–2918.

14 N. Murakami, Y. Tango, H. Miyake, T. Tajima, Y. Nishina, W. Kurashige, Y. Negishi and Y. Takaguchi, *Sci. Rep.*, 2017, **7**, 43445.

15 H. Wang, Y. Yuan, L. Wei, K. Goh, D. S. Yu and Y. Chen, *Carbon*, 2015, **81**, 1–19.

16 F. Yang, X. Wang, M. Li, X. Liu, X. Zhao, D. Zhang, Y. Zhang, J. Yang and Y. Li, *Acc. Chem. Res.*, 2016, **49**, 606–615.

17 S. Zhang, L. Kang, X. Wang, L. Tong, L. Yang, Z. Wang, K. Qi, S. Deng, Q. Li, X. Bai, F. Ding and J. Zhang, *Nature*, 2017, **543**, 234–238.

18 C. Liu and H.-M. Cheng, *J. Am. Chem. Soc.*, 2016, **138**, 6690–6698.

19 M. Li, X. Liu, X. Zhao, F. Yang, X. Wang and Y. Li, *Top. Curr. Chem.*, 2017, **375**, 29.

20 S. M. Bachilo, L. Balzano, J. E. Herrera, F. Pompeo, D. E. Resasco and R. B. Weisman, *J. Am. Chem. Soc.*, 2003, **125**, 11186–11187.

21 G. Lolli, L. Zhang, L. Balzano, N. Sakulchaicharoen, Y. Tan and D. E. Resasco, *J. Phys. Chem. B*, 2006, **110**, 2108–2115.

22 M. He, A. I. Chernov, P. V. Fedotov, E. D. Obraztsova, J. Sainio, E. Rikkinen, H. Jiang, Z. Zhu, Y. Tian and E. I. Kauppinen, *J. Am. Chem. Soc.*, 2010, **132**, 13994–13996.

23 X. Li, X. Tu, S. Zaric, K. Welsher, W. S. Seo, W. Zhao and H. Dai, *J. Am. Chem. Soc.*, 2007, **129**, 15770–15771.

24 K. Cui, A. Kumamoto, R. Xiang, H. An, B. Wang, T. Inoue, S. Chiashi, Y. Ikuhara and S. Maruyama, *Nanoscale*, 2016, **8**, 1608–1617.

25 M. He, B. Liu, A. I. Chernov, E. D. Obraztsova, I. Kauppi, H. Jiang, I. Anoshkin, F. Cavalca, T. W. Hansen, J. B. Wagner, A. G. Nasibulin, E. I. Kauppinen, J. Linnekoski, M. Niemelä and J. Lehtonen, *Chem. Mater.*, 2012, **24**, 1796–1801.

26 F. Yang, X. Wang, D. Zhang, J. Yang, D. Luo, Z. Xu, J. Wei, J.-Q. Wang, Z. Xu, F. Peng, X. Li, R. Li, Y. Li, M. Li, X. Bai, F. Ding and Y. Li, *Nature*, 2014, **510**, 522–524.

27 F. Yang, X. Wang, D. Zhang, K. Qi, J. Yang, Z. Xu, M. Li, X. Zhao, X. Bai and Y. Li, *J. Am. Chem. Soc.*, 2015, **137**, 8688–8691.

28 F. Yang, X. Wang, J. Si, X. Zhao, K. Qi, C. Jin, Z. Zhang, M. Li, D. Zhang, J. Yang, Z. Zhang, Z. Xu, L. M. Peng, X. Bai and Y. Li, *ACS Nano*, 2017, **11**, 186–193.

29 H. An, A. Kumamoto, H. Takezaki, S. Ohyama, Y. Qian, T. Inoue, Y. Ikuhara, S. Chiashi, R. Xiang and S. Maruyama, *Nanoscale*, 2016, **8**, 14523–14529.

30 M. Li, F. Yang, L. Ding, X. Liu, Z. Zhang, D. Zhang, X. Zhao, J. Yang and Y. Li, *Carbon*, 2017, **118**, 485–492.

31 Y. Li, R. Cui, L. Ding, Y. Liu, W. Zhou, Y. Zhang, Z. Jin, F. Peng and J. Liu, *Adv. Mater.*, 2010, **22**, 1508–1515.

32 D. Zhang, J. Yang, F. Yang, R. Li, M. Li, D. Ji and Y. Li, *Nanoscale*, 2015, **7**, 10719–10727.

33 M. S. Dresselhaus, G. Dresselhaus, R. Saito and A. Jorio, *Phys. Rep.*, 2005, **409**, 47–99.

34 K. Liu, X. Hong, Q. Zhou, C. Jin, J. Li, W. Zhou, J. Liu, E. Wang, A. Zettl and F. Wang, *Nat. Nanotechnol.*, 2013, **8**, 917–922.

35 Y. C. Kimmel, D. V. Esposito, R. W. Birkmire and J. G. Chen, *Int. J. Hydrogen Energy*, 2012, **37**, 3019–3024.

36 S. T. Hunt, T. Nimmanwudipong and Y. Román-Leshkov, *Angew. Chem., Int. Ed.*, 2014, **53**, 5131–5136.

37 V. Keller, P. Wehrer, F. Garin, R. Ducros and G. Maire, *J. Catal.*, 1995, **153**, 9–16.

38 V. Keller, P. Wehrer, F. Garin, R. Ducros and G. Maire, *J. Catal.*, 1997, **166**, 125–135.

39 J. F. Moulder, W. F. Stickle, P. E. Sobol and K. D. Bomben, *Handbook of X-ray Photoelectron Spectroscopy*, Physical Electronics, Inc., 6509 Flying Cloud Drive Eden, Minnesoda 55344, United States of America, 1995.

40 B. Wang, C. H. P. Poa, L. Wei, L. J. Li, Y. Yang and Y. Chen, *J. Am. Chem. Soc.*, 2007, **129**, 9014–9019.

41 B. Wang, L. Wei, L. Yao, L. J. Li, Y. Yang and Y. Chen, *J. Phys. Chem. C*, 2007, **111**, 14612–14616.

42 B. Yu, C. Liu, P.-X. Hou, Y. Tian, S. Li, B. Liu, F. Li, E. I. Kauppinen and H.-M. Cheng, *J. Am. Chem. Soc.*, 2011, **133**, 5232–5235.

43 X. Qin, F. Peng, F. Yang, X. He, H. Huang, D. Luo, J. Yang, S. Wang, H. Liu, L. Peng and Y. Li, *Nano Lett.*, 2014, **14**, 512–517.

44 W. Zhou, S. Zhan, L. Ding and J. Liu, *J. Am. Chem. Soc.*, 2012, **134**, 14019–14026.